PROCEEDINGS, 50th Workshop on Geothermal Reservoir Engineering
Stanford University, Stanford, California, February 10-12, 2025
SGP-TR-229

A Unified Compositional Flow Model for Simulating Multiphase High-Enthalpy Geothermal Reservoirs

Micheal Oguntola[1,2], Omar Duran[1], Veljko Lipovac[1], Eirik Keilegavlen[1] and Inga Berre[1]

[1]University of Bergen, Bergen, Norway

[2]micheal.oguntola@uib.no

Keywords: geothermal simulator, compositional flow model, phase-transition, high-enthalpy simulation, non-isothermal flow

ABSTRACT

Simulating high-enthalpy geothermal reservoirs poses significant challenges due to the complex interactions between multicomponent, multiphase geothermal fluids influenced by varying pressure, temperature, and other physical conditions. These complexities complicate the development of models that can efficiently quantify the impact of production strategies and other aspects relevant to the engineering of geothermal systems. In this work, we propose a unified compositional flow model for geothermal reservoir simulation, which integrates mass and energy conservation laws across predefined phases, advanced equations of state (EOS), and a comprehensive thermodynamic framework. This unified formulation maintains a persistent set of unknowns and equations, and efficiently manages phase transitions using complementarity conditions. This approach eliminates the need for manual phase switching, enhancing both numerical stability and computational efficiency. Our model captures essential phase behaviors and allows a general, thermodynamically consistent representation of fluid properties, crucial for the development and operation of geothermal reservoirs. Implemented within the open-source, Python-based framework PorePy, we verify our model through numerical experiments simulating various geothermal reservoir conditions. The results present valuable insights into phase transitions, heat transfer, and component transport and show strong agreement with key benchmark simulations from the commercial geothermal simulator CSMP++.

1. INTRODUCTION

Geothermal reservoirs, especially those in high-enthalpy settings, are low-carbon sources of renewable energy. Recent estimates show that high-enthalpy geothermal reservoirs contribute a capacity of approximately 16319 MW for global power and heat generation, making a significant contribution to renewable energy integration while reducing reliance on fossil fuels, with capacity expected to grow in the future (Luis C. A, 2024; Richter, 2023; Sabine et al., 2008). To improve and optimize operational performance, it is profitable to accurately understand subsurface dynamics of these reservoirs.

High-enthalpy geothermal reservoirs are often situated in inaccessible regions of the Earth's crust, associated with magmatic activity, which makes data acquisition challenging and limits our understanding of subsurface dynamics. They also exhibit complex behaviors driven by multicomponent multiphase geothermal fluids, typically consisting of liquid water, steam, and dissolved gases and minerals, which interact under varying pressure, temperature, and other physical conditions. For example, extreme temperature gradients can induce phase separation between liquid and vapor phases, while near-critical conditions can lead to sharp variations in fluid thermodynamic properties and abrupt phase transitions (Abdulagatov et al., 2020, 2021). Also, high salinity may lead to mineral precipitation, such as silica or calcite, within fractures, thus altering fluid flow paths and matrix permeability (Reinsch et al., 2017). Several numerical modeling and simulation techniques have been devised to simulate high-enthalpy systems with the aim of addressing specific challenges associated with these systems. Review studies by Ingebritsen et al. (2010) examined the formulations of a range of geothermal numerical simulators, including TOUGH2 (Pruess, 1991, 2003), HYDROTHERM (Kipp et al., 2008), CSMP++ (Geiger et al., 2006a, 2006b; Weis et al., 2014), FISHES (Lewis & Lowell, 2009), and FEHM (Zyvoloski et al., 1997), as well as their limitations in terms of capabilities and allowable pressure and temperature bounds. Additionally, other existing simulators, such as FALCON (Podgorney et al., 2010; Xia et al., 2017), ComPASS (Les Landes et al., 2025; Lopez et al., 2018), and DARTS (Khait, 2019; Wang et al., 2020), have further contributed to the expanding suite of numerical tools available for geothermal reservoir modeling.

In modelling multiphase flow and transport within geothermal reservoirs, an accurate representation of the fluid phase composition is crucial for capturing the complex underlying physical processes. Similar challenges arise in fields such as oil reservoir simulation (Chen et al., 2006) and CO_2 sequestration (Bert et al., 2005). A key difficulty in these multiphase, multicomponent models (also known as compositional models) is quantifying phase transitions and the corresponding changes in fluid properties, as fluid phase appearance or disappearance locally alters the system's physics, introducing strong nonlinearities into the governing equations (Lauser et al., 2011). Without appropriate incorporation of these transitions in the compositional model, governed by non-linear system of partial differential equations (PDEs), solution techniques for the governing PDEs may experience numerical instabilities (Class & Helmig, 2002).

Phase transitions in compositional models are addressed through different approaches, each developed to meet modeling needs and applications; for examples and details, refer to the studies by Aghili et al. (2020), Beaude et al. (2019), Bui & Elman (2020), Gharbia et al. (2021), Lauser et al. (2011), Quiroz et al. (2024), and Rajabi & Chen (2023). One commonly used approach is variable switching,

which dynamically adjusts the set of unknowns based on the phase distribution at specific spatial points in time. In this approach, the variables are redefined based on the present phases, allowing for computational efficiency in terms of the size of equations (or equivalently, number of unknowns) that is solved per time, especially in scenarios with frequent phase transitions (Alpak & Vink, 2018; Beaude et al., 2019). However, this method may face convergence issues near phase boundaries, demanding robust handling to avoid numerical oscillations (Class & Helmig, 2002). Alternatively, a persistent variable method (also known as unified formulation) offers a fixed set of unknowns and equations throughout the simulation model, regardless of phase presence or absence. This approach eliminates the need for variable switching by combining natural physical quantities (Voskov & Tchelepi, 2012) with local equilibrium-based extensions to simplify the numerical treatment of phase transitions and enhance numerical stability (Falko et al., 2021; Gharbia et al., 2021; Lauser et al., 2011; Weis et al., 2014). While this method is generally less computationally intensive in nonlinear systems, it requires complementarity constraints to ensure accuracy in phase transition handling. In this context, typical formulations often adopted in state-of-the-art geothermal simulators include the pressure-temperature variable switching approach employed in TOUGH2 (Pruess, 2003), and the pressure-enthalpy formulation used in HYDROTHERM (Kipp et al., 2008). Additionally, the space-time flow and transport equations can be solved either simultaneously, as in HYDROTHERM or by employing operator-splitting approaches, such as the sequential coupling of flow and transport equations implemented in CSMP++ (Weis et al., 2014).

In this work, we present a numerical model for simulating high-enthalpy geothermal reservoirs built upon a unified compositional model that employs a persistent set of primary variables and equations. The framework incorporates advanced equations of state to represent the thermodynamic properties and behavior of multicomponent fluids and is implemented within the open-source, Python-based PorePy platform (Keilegavlen et al., 2021). Through a series of benchmark simulations, including comparisons with the commercial geothermal simulator CSMP++ (Weis et al., 2014), the model demonstrates its capability to accurately simulate phase transitions, heat transfer, and component transport within high-enthalpy geothermal systems.

2. MODEL FORMULATION

This section describes the mathematical and thermodynamic framework underlying our unified compositional model for simulating a high-enthalpy geothermal reservoir. We begin by outlining the model assumptions, followed by the governing equations for mass and energy conservation of components and phases within the reservoir, forming the foundation of the compositional model. Subsequently, we introduce the thermodynamic framework employed to capture the multicomponent, multiphase behavior of geothermal fluids.

2.1 Model Assumptions

For the numerical experiments performed in this work, we consider the following model assumptions:

- capillary pressure effects are neglected
- no chemical reactions between components
- there is mass transfer between existing phases
- hydrodynamic dispersion and components diffusion are neglected
- geothermal rock and fluid are in local thermal equilibrium
- conservation of momentum is described by the multiphase Darcy law
- gravity is neglected.

2.1 Governing Equations

Considering the geothermal reservoir as a multicomponent, multiphase continuum porous medium, we assume that the reservoir contains N_c different components, indexed by $\xi \in \{1,2,\dots,N_c\}$, which can coexist as N_p different phases, indexed by $\gamma \in \{1,2,\dots,N_p\}$. Under the assumption of no capillary pressure, we have $p_\gamma = p, \forall \gamma$, where p is the uniform pressure across phases. Additionally, the assumption of local thermal equilibrium implies that $T_\gamma = T_s = T, \forall \gamma$, where T_s and T represent the solid rock and fluid temperatures, respectively. By applying the general conservation law in combination with the model assumptions, we derive the balance equations for each component, pressure, and energy using fractional flow formulation (for a definition of the fractional flow formulation, see Duran et al. (2025)). The choice of fractional formulation is made to permit the reusability of code, especially for the discretization of diffusive terms in the governing equations. Additionally, representing the overall mass flux as a continuous variable facilitates the use of sequential schemes. An extension of the model to fractured media, including gravity effect, is given in Duran et al. (2025). The definitions and units of variables and parameters are stated in Tables 1-3.

2.1.1 Balance equation of overall mass of component

For each component $\xi \in \{1,2,\dots,N_c\}$, the balance equation of overall mass z_ξ of the component is given by:

$$\frac{\partial(\phi \rho z_\xi)}{\partial t} + \nabla \cdot \left[f_\xi \lambda \, \underline{\boldsymbol{K}} \nabla p \right] = \mathrm{q}_\xi, \tag{1}$$

where ϕ is the porosity, $\underline{\boldsymbol{K}}$ is the permeability tensor, and the component fractional flow f_ξ is defined as:

$$f_\xi = \frac{\lambda_\xi}{\lambda}. \tag{2}$$

The density-weighted mobility of component ξ in phase γ is given by:

$$\lambda_{\xi\gamma} = \frac{\rho_\gamma \chi_{\xi\gamma}\, k_{r\gamma}}{\mu_\gamma}, \tag{3}$$

so that, using Equation (3), the density-weighted mobility λ_ξ of component ξ and the total density-weighted mobility λ, respectively, are derived as:

$$\lambda_\xi = \sum_{\gamma=1}^{N_p} \frac{\rho_\gamma \chi_{\xi\gamma}\, k_{r\gamma}}{\mu_\gamma}, \qquad \lambda = \sum_{\xi=1}^{N_c} \lambda_\xi. \tag{4}$$

The fluid mixture density ρ is expressed as:

$$\rho = \sum_{\gamma\,=\,1}^{N_p} s_\gamma \rho_\gamma\,. \tag{5}$$

Mathematically, the physical quantity z_ξ can also be expressed as:

$$z_\xi = \sum_{\gamma\,=\,1}^{N_p} y_\gamma \chi_{\xi\gamma}\,, \tag{6}$$

where $y_\gamma = \frac{1}{\rho}\sum_\gamma \rho_\gamma s_\gamma$ is the mass fraction of phase γ in the fluid mixture. Substituting Equations (2) – (6) into (1), we arrive at a similar balance equation for components in (Lauser et al., 2011; Weis et al., 2014).

2.1.2 Balance equation of total mass

By summing both sides of Equation (1) over all components ξ and assuming mass conservation, we obtain:

$$\sum_{\xi=1}^{N_c}\left(\frac{\partial\left(\phi\rho z_\xi\right)}{\partial t} + \nabla\cdot\left[f_\xi \lambda\, \underline{\boldsymbol{K}}\nabla p\right]\right) = \sum_{\xi=1}^{N_c} q_\xi \implies \frac{\partial(\phi\rho)}{\partial t} + \nabla\cdot\left[\lambda\, \underline{\boldsymbol{K}}\nabla p\right] = q\,. \tag{7}$$

Equation (7) holds true because, from Equations (2) and (6), we have $\sum_\xi f_\xi = 1$ and $\sum_\xi z_\xi = 1$, respectively, and $q = \sum_\xi q_\xi$. The total density-weighted mobility λ and fluid density ρ are given by Equations (4) and (5) respectively. In porous media flow, Equation (7) is commonly called the pressure or flow equation (Chen et al., 2006).

2.1.3 Balance equation of energy

The energy conservation equation in terms of the specific enthalpy of fluid mixture is expressed as follows:

$$\frac{\partial}{\partial t}(\phi[\rho h - p] + (1-\phi)\rho_s h_s) - \nabla\cdot\left(\sum_\gamma \lambda_\gamma h_\gamma \underline{\boldsymbol{K}}\nabla p + \underline{\boldsymbol{D}}_h \nabla T\right) = q_e, \tag{8}$$

where the specific enthalpy of the fluid mixture $h = \sum_\gamma y_\gamma h_\gamma$ and the specific enthalpy of rock $h_s = c_{ps}T$. The thermal conductivity tensor $\underline{\boldsymbol{D}}_h = \left(\phi\sum_\gamma s_\gamma \kappa_\gamma + (1-\phi)\kappa_s\right)\underline{\boldsymbol{I}}_d$. The mobility λ_γ of phase γ is obtained by summing over all components in Equation (3), i.e., $\lambda_\gamma = \sum_\xi \frac{\rho_\gamma \chi_{\xi\gamma}\, k_{r\gamma}}{\mu_\gamma}$.

2.1.4 Choice of primary variables

Equations (1) - (8) form a strongly coupled system of time-dependent, non-linear partial differential and algebraic equations. In total, there are $N_c + 2$ equations for $N_c N_p + 2N_p + N_c + 3$ independent variables (see Tables 1 and 2). We note here that there are more independent variables than the number of equations, resulting in an underdetermined system. To achieve a unique solution, it is necessary to introduce $N_c N_p + 2N_p + N_c + 3$ independent equations. Typically, additional equations required to close the system are derived from constitutive laws such as the assumption of local phase equilibrium conditions imposed on designated set of primary variables (see the next Subsection). The resulting phase equilibrium relations are equivalent to minimizing the Gibbs free energy of the geothermal compositional system (Chen et al., 2006).

The selection of primary variables defining the thermodynamic state of the compositional system requires careful consideration. For example, in a salt-water multiphase system, the use of p, T, z_1, z_2 as the primary variables requires additional treatment to appropriately resolve phase saturations in energetic states because of latent heat of vaporization (see, e.g., Geiger et al. (2006)). For this reason, we consider the primary variables presented in Table 1. The set of primary variables is denoted as $\boldsymbol{x} = \{p, h, z_1, \ldots, z_{N_c}\}$.

Table 1: Definitions of primary variables

Variable	Meaning	Units
z_ξ	Overall mass fraction of component $\xi \in \{1,2,..,N_c\}$	−
p	Pressure	Pa
h	Specific enthalpy of fluid mixture	J/kg

2.1.4 Constitutive relations

We present algebraic constraints derived from constitutive laws (Chen et al., 2006) to close the system of differential equations (1), (7), and (8). First, the overall mass fractions of components must satisfy:

$$\sum_{\xi=1}^{N_c} z_\xi = 1. \tag{9}$$

Additionally, independent equations, also known as secondary equations, based on the primary variables in Table l are introduced to eliminate the $N_p N_c + 2N_p + 1$ secondary variables given in Table 2. We denote the set of secondary variables as $\boldsymbol{y_x}$, where the subscript $\boldsymbol{x}$ indicates that their selection depends on the choice of $\boldsymbol{x}$.

In the context of transport processes, the geothermal reservoir is saturated with different fluid phases such that

$$\sum_{\gamma=1}^{N_p} s_\gamma = 1 \quad \text{and} \quad \sum_{\gamma=1}^{N_p} y_\gamma = 1\,. \tag{10}$$

Within each phase $\gamma \in \{1,2,\dots,N_p\}$, the partial fractions of components present in the phase, i.e., $\chi_{\xi\gamma}, \forall \xi \in \{1,2,\dots,N_c\}$ satisfy:

$$\sum_{\xi=1}^{N_c} \chi_{\xi\gamma} = 1\,. \tag{11}$$

To model phase behavior, phase equilibrium relations subject to complementarity inequality constraints are usually employed (Gharbia et al., 2021; Lauser et al., 2011; Lipovac et al., 2023). This is also called flash calculation. At each point in the $\boldsymbol{x}$ – space, these inequality relations are solved for the presence and composition of phases in the system. This makes the solution of the compositional model computationally expensive. To reduce this computational cost, Voskov (2017) introduced an operator-based linearization (OBL) model that precomputes flash calculations at a limited set of points in the $\boldsymbol{x}$-space enough to cover the boundary points of interest. Flash data for other points are then estimated through interpolation, significantly increasing computational efficiency.

In our approach, we also interpolate flash data using precomputed flash calculations on selected points in the $\boldsymbol{x}$ – space. Unlike in (Voskov, 2017), where the flash problem is numerically solved, our flash calculations are based on the correlation formulas developed by Driesner & Christoph (2007). For a binary salt-water system, these correlations provide a consistent formulation for phase behavior across a wide range of geothermal conditions, specifically for $p \in [0, 5000]$ bar, $T \in [0, 1000]^o$C, and overall salt fraction $z \in [0, 1]$. We rely on and further extend the C++-library swEOS, which implements these correlations (Guo & Rüpke, 2021). Falko et al. (2021) and Weis et al. (2014) utilized similar correlation-based flash approaches to simulate different geothermal applications.

Table 2: Definitions of secondary variables

Variable	Meaning	Unit
s_γ	Volumetric saturation of phase $\gamma \in \{1,2,..,N_p\}$	−
T	Temperature	K
$\chi_{\xi\gamma}$	Partial fraction of component $\xi \in \{1,2,\dots,N_c\}$ in phase $\gamma \in \{1,2,\dots,N_p\}$	−
y_γ	Fraction of phase $\gamma \in \{1,2,\dots,N_p\}$ in the fluid mixture	−

Remark 1. Assume that $N_c \geq 2$ and $N_p \geq 2$, with component N_c and phase N_p chosen as references. The overall fraction of the reference component can be eliminated using the algebraic Equation (9), thereby reducing the number of PDEs in Equation (1) that needs to be solved. Also, thermodynamic properties of the reference phase, such as its saturation, fraction, and partial fraction of the reference component, can be eliminated using Equations (10) and (11) respectively.

Remark 2. Some of the quantities listed in Table 3, such as ϕ, are given constants. Others, like ρ_γ are computed dynamically from suitable equations of thermodynamic state variables $\boldsymbol{x}$ and/ or secondary variables $\boldsymbol{y_x}$, e.g., IAPWS-97. In this work, we focus on utilizing the saltwater equation of state combined with mixture rules.

Table 3: List of other physical quantities (Definitions and values used in this study)

Variable	Meaning	Value	Unit
ϕ	Porosity of rock	0.1	–
ρ	Fluid mixture density		kg/m^3
ρ_γ	Density of phase γ		kg/m^3
ρ_s	Density of solid rock	2750	kg/m^3
$\underline{\boldsymbol{K}}$	Isotropic absolute permeability tensor of porous medium		m^2
q_ξ	Source/sink term for component ξ	0.0	kgm^{-3}s^{-1}
q_e	Source/ sink term for energy flux	0.0	Jm^{-1}s^{-1}
$k_{r\gamma}$	Relative permeability of phase γ		–
μ_γ	Viscosity of phase γ		Pa.s
$\lambda_{\xi\gamma}$	Density-weighted mobility of component ξ in phase γ		Pa^{-1}.s
λ_ξ	Density-weighted mobility of component ξ		Pa^{-1}.s
λ	Total density-weighted mobility of fluid mixture of components or phases		Pa^{-1}.s
$\underline{\boldsymbol{I}}_d$	Identity matrix of size d		–
h_γ	Specific enthalpy of phase γ		J/kg
κ_γ	Thermal conductivity of phase γ	2.0	Wm^{-1}K^{-1}
κ_s	Thermal conductivity of solid rock	2.0	Wm^{-1}K^{-1}
c_{ps}	Specific heat capacity of solid rock	880	Jkg^{-1}K^{-1}
$\underline{\boldsymbol{D}}_h$	Absolute thermal conductivity tensor		Wm^{-1}K^{-1}

3. NUMERICAL SOLUTION

Consider a geothermal reservoir as a continuum represented by a bounded and open domain $\Omega \subset R^d$, where $d = 1,2, or\ 3$ denotes the spatial dimension and R is the set of real numbers. Let $\partial\Omega$ be the boundary of Ω, and consider a time interval $[0, \mathcal{T}]$ over which we study the dynamics of the reservoir. The mathematical problem is to find the distribution of the state vector:

$$\begin{aligned} \boldsymbol{X}&: \Omega \times [0,\mathcal{T}] \longrightarrow R^{|\boldsymbol{X}|} \\ (\omega, t) &\longmapsto \boldsymbol{X}(\omega, t) := \begin{pmatrix} \boldsymbol{x}(\omega,t) \\ \boldsymbol{y_x}(\omega,t) \end{pmatrix}, \end{aligned} \tag{12}$$

which satisfies the governing equations (including balance equation of components, pressure, and energy and constitutive relations) in Subsection 2.1, subject to suitable initial conditions $\boldsymbol{X}(\omega, 0) = \boldsymbol{X}_0,\ \omega \in \Omega$ and boundary conditions $\boldsymbol{X}(\omega, t) = \boldsymbol{X}_b,\ \omega \in \partial\Omega$ and $t \in [0, \mathcal{T}]$. Here, $\boldsymbol{x}$ represents the primary variables (see Table 1), $\boldsymbol{y_x}$ represents the secondary variables (see Table 2), and $|\boldsymbol{X}|$ denotes the size of the vector $\boldsymbol{X}$.

Due to the complexity of the coupled, strongly non-linear partial differential equations (1), (7), and (8), it is analytically impossible to determine $\boldsymbol{X}(\omega, t)$. Consequently, we seek an approximate solution using numerical methods.

To illustrate the numerical method used in this work, we start by rewriting the governing equations in Subsection 2.1 in vector form as

$$\frac{\partial \underline{\Xi} \boldsymbol{X}}{\partial t} = \boldsymbol{\mathcal{F}}(t, \omega, \boldsymbol{X}, \boldsymbol{X}_{\omega}, \boldsymbol{X}_{\omega\omega}), \tag{13}$$

where $\underline{\Xi}$ is a sparse, square matrix of size $|\boldsymbol{X}|$ with non-zero entries consisting physical quantities in the accumulation terms. The zero rows correspond to non-PDE components derived from constitutive relations. The vector $\boldsymbol{\mathcal{F}}$ encapsulates fluxes, constitutive relations, and source terms as function of time t, spatial location ω, state vector $\boldsymbol{X}$, spatial derivatives of $\boldsymbol{X}$, specifically $\boldsymbol{X}_{\omega}$(first derivatives) and $\boldsymbol{X}_{\omega\omega}$ (second derivatives).

To approximate the solution of Equation (13), we employ a fully implicit time-stepping scheme that ensures stability when solving stiff non-linear differential equations. Let Δt denote the time step size, we discretize Equation (14) with respect to time, using the implicit Euler method, to arrive at

$$\frac{\left(\underline{\Xi}\boldsymbol{X}\right)_{t+\Delta t} - \left(\underline{\Xi}\boldsymbol{X}\right)_{t}}{\Delta t} = \boldsymbol{\mathcal{F}}_{t+\Delta t}\,. \tag{14}$$

For spatial discretization of Equation (14), we use the multipoint flux approximation (MPFA) finite volume method with a first order upwinding scheme for the advective terms over a predetermined set of partitions (control volumes) of the domain Ω (Aavatsmark, 2002; Chen et al., 2006). The resulting discretized system of nonlinear equations becomes:

$$\boldsymbol{G}(\widehat{\boldsymbol{X}}_{t+\Delta t}) = \boldsymbol{0}, \tag{15}$$

where $\widehat{\boldsymbol{X}}_{t+\Delta t}$ is the discrete state vector, which includes all primary and secondary variables at each control volume at time $t + \Delta t$. Specifically, if N is the total number of control volumes, the size of $\widehat{\boldsymbol{X}}_{t+\Delta t}$ becomes $\mathrm{N}|\boldsymbol{X}|$. To solve the non-linear system in Equation (16), we use Newton method, which linearizes the system around the current estimate $\mathbf{X}_{\mathrm{t+\Delta t}}^{(\mathrm{n})}$ at iteration n to get

$$\boldsymbol{J}\left(\widehat{\boldsymbol{X}}_{t+\Delta t}^{(n)}\right)\Delta\widehat{\boldsymbol{X}}^{(n)} = -\boldsymbol{G}\left(\widehat{\boldsymbol{X}}_{t+\Delta t}^{(n)}\right), \tag{16}$$

where $\boldsymbol{J}$ is the Jacobian matrix of $\boldsymbol{G}$ and $\Delta\widehat{\boldsymbol{X}}^{(n)} = \widehat{\boldsymbol{X}}_{t+\Delta t}^{(n+1)} - \widehat{\boldsymbol{X}}_{t+\Delta t}^{(n)}$ is the Newton update. Equation (16) is solved for $\Delta\widehat{\boldsymbol{X}}^{(n)}$ using suitable direct linear solver. The solution is then updated as

$$\widehat{\boldsymbol{X}}_{t+\Delta t}^{(n+1)} = \widehat{\boldsymbol{X}}_{t+\Delta t}^{(n)} + \Delta\widehat{\boldsymbol{X}}^{(n)}, \qquad \text{for all } n = 0,1,2,\ldots, \tag{17}$$

and the iterative process continues until convergence is achieved for $\widehat{\boldsymbol{X}}_{t+\Delta t}$. In this study, convergence at a given iterate $\widehat{\boldsymbol{X}}_{t+\Delta t}^{(n)}$ is reached when the l_2-norm of the residual $\boldsymbol{G}(\widehat{\boldsymbol{X}}_{t+\Delta t}^{(n)})$ falls below a predefined tolerance $0 \leq \epsilon \leq 10^{-10}$.

The solution strategy is implemented within the Python-based PorePy framework (Keilegavlen et al., 2021). PorePy is an open-source simulation tool designed for solving multiphysics problems in fractured porous media. Within PorePy, the domain discretization into control volumes is handled automatically, allowing for integration of complex geometries and heterogeneous material properties.

4. BENCHMARKS

In this section, we present benchmark simulation results to validate the accuracy of our numerical model. These benchmark cases, derived from Weis et al. (2014), are widely used to evaluate geothermal reservoir simulation models (see, e.g., Copol et al. (2014) and Guo et al. (2020)). For verification, our results are compared with those from CSMP++, a commercial multiphysics simulation toolbox developed for geothermal reservoir modeling. CSMP++ employs a semi-implicit sequential approach combined with a finite-element finite-volume discretization scheme to separately handle the different components of the advection-diffusion flow and transport equations (Geiger et al., 2006a; Weis et al., 2014). In contrast, our approach utilizes a fully implicit scheme coupled with a multipoint flux approximation (MPFA) finite-volume method. In all cases, our model shows strong agreement with CSMP++ results.

4.1 One-dimensional simulations

We conducted five 1-D simulations of a single pure-water component ($N_c = 1$) in a horizontally oriented domain with a length of 2 km, as shown in Figure 1. The entire simulation setup, including domain configuration, initial and boundary conditions, and rock and fluid parameter choices, is adopted directly from Weis et al. (2014) for consistency and comparability. The grid spacing is set to 10 m, and the simulations are configured with Dirichlet boundary conditions, maintaining constant temperature and pressure conditions on both ends of the domain. In the absence of gravity, higher p-T values are considered on the left boundary than the right, creating a pressure gradient that drives flow from left to right. The initial temperature is set to the downstream boundary temperature, while the initial pressure is linearly distributed, as shown in Figure 1. The domain is initially liquid dominated. In all experiments, the Newton convergence tolerance is set to $\epsilon = 1.0 \times 10^{-4}$.

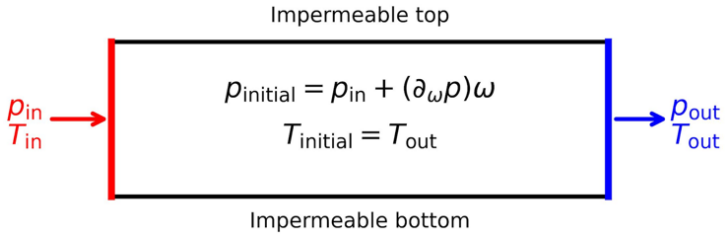

Figure 1: Schematic representation of a 1-D liquid-dominated domain with Dirichlet boundary conditions at both ends and the specified initial conditions for temperature and pressure. p_{in}, p_{out}, T_{in}, **and** T_{out} **are the inlet and outlet pressure and temperature values respectively,** $\partial_\omega p$ **is the pressure gradient in the domain, and** p_{initial} **and** T_{initial} **are the initial pressure and temperature profiles**

4.1.1 Single-phase flow

In this experiment, we considered boundary conditions that allow for the flow of a single fluid phase within the domain. Three different cases are examined: Liquid Phase, Supercritical Fluid, and Vapor Phase, as depicted in Figure 2. The relative permeability of each phase is linearly set to the phase saturation. The same time step size, $\Delta t = 365$ days for all cases, consistent with the CSMP++ simulations is used. The progression of the thermal font and pressure profile in each case with different simulation periods compared with results from the reference simulator are reported in Figure 2. Here, we see that the results from the two simulators are almost identical.

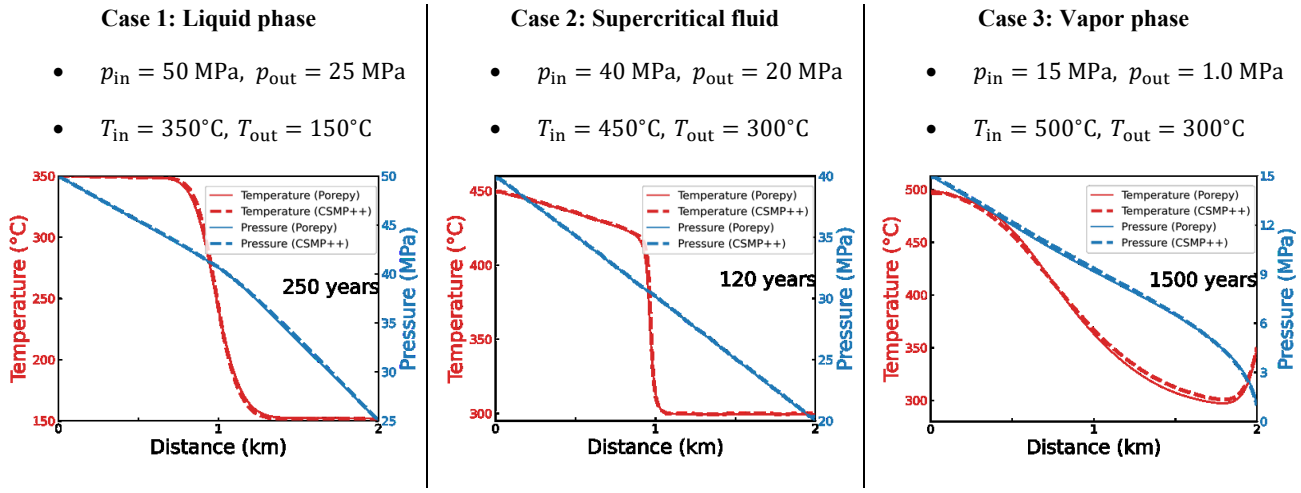

Figure 2: Snapshots of single-phase, one-dimensional simulations of a heating thermal front in horizontal orientation for three different test cases. Results for fluid pressure (blue) and temperature (red) from PorePy are plotted as dashed lines, results from CSMP++ as dashed lines.

4.1.2 Two-phase flow

To allow for two-phase (liquid and vapor) flow in the domain, we simulated the injection of hot steam at 400^oC into an initially 150^oC liquid-dominated domain at a fixed fluid pressure values of 20 MPa and 1 MPa at the left and right boundaries respectively. In this case, the residual saturation of the liquid phase is set to $R_l = 0.3$ (as indicated by the dashed dark lines in Figure 3 and 4). This value represents the saturation at which the relative permeability of the liquid phase is zero, and the liquid phase becomes immobile. For the vapor phase, the residual saturation is set to $R_v = 0.0$, which allows vapor to be mobile throughout the domain. Consequently, the relative permeability relations for the liquid and vapor phases are defined as:

$$k_{rl} = \begin{cases} 0 & \text{if } s_l \le R_l \\ \dfrac{s_l - R_l}{1 - (R_l + R_v)} & \text{if } s_l > R_l \end{cases}, \quad k_{rv} = \frac{s_v - R_v}{1 - (R_l + R_v)}.$$

The time step size, $\Delta t = 100$ days. The hot steam injection is simulated over a total duration of 200 years. The resulting temperature, pressure, and liquid saturation profiles from the PorePy and CSMP++ simulators are presented in Figure 3. In this case, the results show a good match, except for a slight difference in the width of the two-phase region. This discrepancy arises from the difference in the solution strategies used by the two simulators. For example, in CSMP++, temperature is considered as a primary variable, requiring additional treatment to handle phase saturations in boiling zones, and dynamic time stepping criteria are employed (Geiger et al., 2006a; Weis et al., 2014).

To extend the evolution of the two-phase region in the above simulation, a smaller pressure gradient is applied by reducing the fluid pressure at the left boundary to 4 MPa, while maintaining the temperature at 300^{o}C. The simulation time is increased to 2000 years, with a time step size of $\Delta t = 365$ days. All other parameter values remain the same as in the previous setup. The resulting temperature, pressure, and liquid saturation profiles from the PorePy and CSMP++ simulators are presented in Figure 4, indicating a good match.

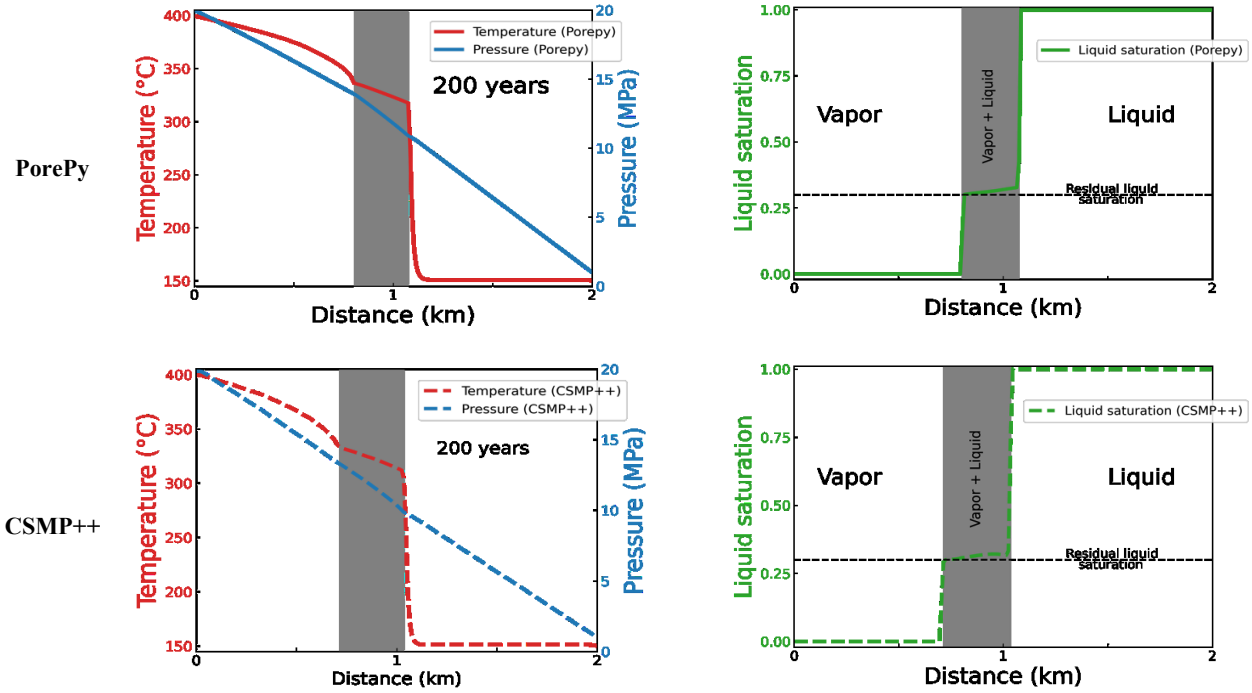

Figure 3: Snapshots of two-phase, one-dimensional simulations with pure water in horizontal orientation. Results for fluid pressure (blue), temperature (red), and liquid saturation (green) from PorePy are plotted on the first row as solid lines, results from CSMP++ on the second row as dashed lines. The grey region represents the two-phase liquid vapor region.

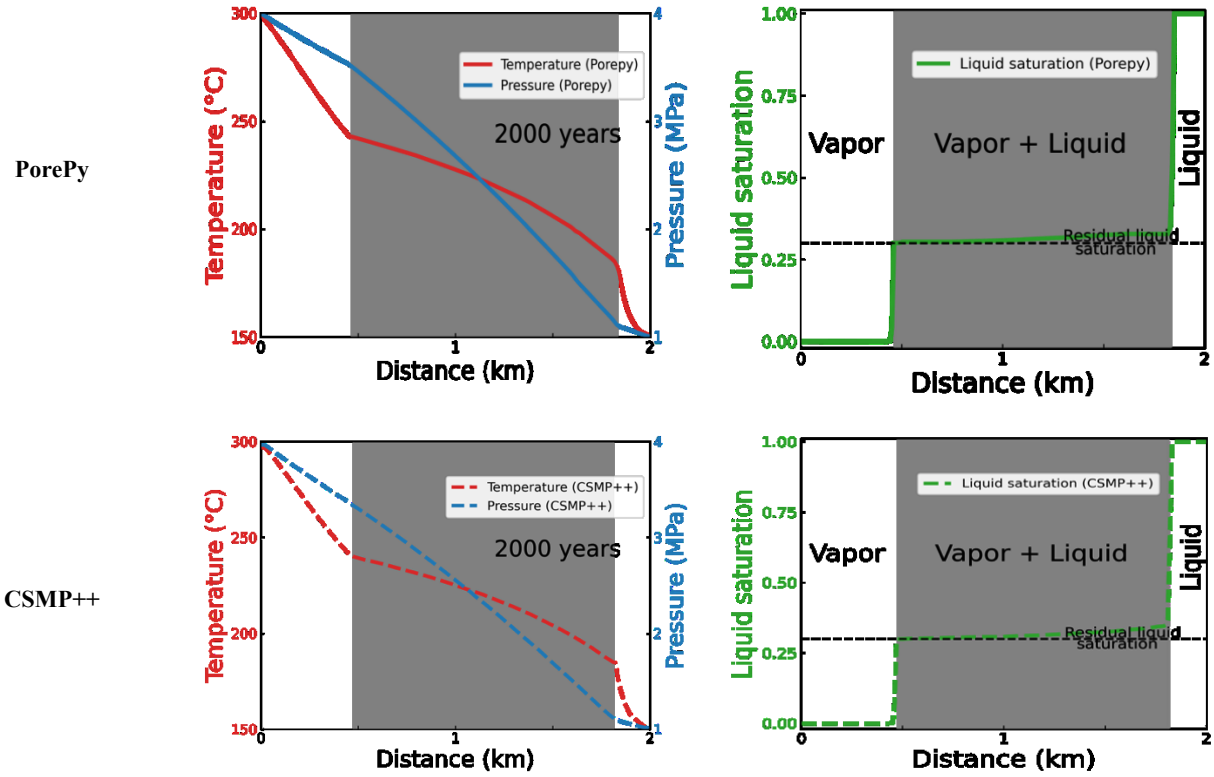

Figure 4: Snapshots of multiphase, one-dimensional simulations. Results for fluid pressure (blue), temperature (red), liquid saturation (green) from PorePy are plotted as solid lines on the first row, results from CSMP++ as dashed lines on the second row. The grey region represents the two-phase liquid vapor region.

6. CONCLUSION

This paper presents a unified compositional numerical model and its capability to simulate high-enthalpy geothermal reservoir conditions. The model has been validated through benchmark simulations involving single pure water component flow in both single-phase and two-phase regimes, to demonstrate its accuracy and robustness.

Future work will focus on extending the model for the simulation of multi-component systems that allow for more complex phase behavior.

DATA AVAILABILITY

The data and source code for the results presented in this work are available, and the plots can be reproduced using a Docker container hosted at: https://doi.org/10.5281/zenodo.14784514 .

ACKNOWLEGMENT

This project has received funding from the European Research Council (ERC) under the European Union's Horizon 2020 research and innovation programme (grant agreement No 101002507).

REFERENCES

Aavatsmark, I. (2002). An introduction to multipoint flux approximations for quadrilateral grids. Computational Geosciences, 6, 405–432.

Abdulagatov, I. M., Скрипов, П. В., & Skripov, P. V. (2020). Thermodynamic and transport properties of supercritical fluids: Review of thermodynamic properties (Part 1). Russian Journal of Physical Chemistry B, 14(7), 1178–1216. https://doi.org/10.1134/s1990793120070192

Abdulagatov, I. M., Скрипов, П. В., & Skripov, P. V. (2021). Thermodynamic and transport properties of supercritical fluids: Review of thermodynamic properties (Part 2). Russian Journal of Physical Chemistry B, 15(7), 1171–1188. https://doi.org/10.1134/s1990793121070022

Aghili, J., Dreuzy, J. de, Masson, R., & Trenty, L. (2020). A hybrid-dimensional compositional two-phase flow model in fractured porous media with phase transitions and Fickian diffusion. Journal of Computational Physics, 441, 110452. https://doi.org/10.1016/j.jcp.2021.110452

Alpak, F. O., & Vink, J. C. (2018). A variable-switching method for mass-variable-based reservoir simulators. Spe Journal, 23(5), 1469–1495. https://doi.org/10.2118/182606-pa

Beaude, L., Brenner, K., Lopez, S., Masson, R., & Smaï, F. (2019). Non-isothermal compositional liquid gas Darcy flow: Formulation, soil-atmosphere boundary condition and application to high-energy geothermal simulations. Computational Geosciences, 23(3), 1–28. https://doi.org/10.1007/s10596-018-9794-9

Bert, M., Ogunlade, D., HC, D. C., Manuela, L., & Leo, M. (2005). IPCC special report on carbon dioxide capture and storage. Cambridge: Cambridge University Press.

Bui, Q. M., & Elman, H. C. (2020). Semi-smooth Newton methods for nonlinear complementarity formulation of compositional two-phase flow in porous media. Journal of Computational Physics, 407, 109163. https://doi.org/10.1016/j.jcp.2019.109163

Chen, Z., Huan, G., & Ma, Y. (2006). Computational methods for multiphase flows in porous media. Philadelphia: SIAM.

Class, H., & Helmig, R. (2002). Numerical simulation of non-isothermal multiphase multicomponent processes in porous media.: 2. Applications for the injection of steam and air. Advances in Water Resources, 25(5PDE), 551--564.

Copol, C., Laminie, J., & Lopez, S. (2014). Numerical modeling of geothermal systems. 39th Workshop on Geothermal Reservoir Engineering, Pp. SGP-TR.

Driesner, T., & Christoph, H. (2007). The system H2O--NaCl. Part I: Correlation formulae for phase relations in temperature-pressure-composition space from 0 to 1000 C, 0 to 5000 bar, and 0 to 1 XNaCl. Geochimica et Cosmochimica Acta, 71(20), 4880--4901.

Duran, O., Lipovac, V., & Berre, I. (2025). A mixed-dimensional approach for compositional multiphase flow in high-enthalpy fractured geothermal reservoirs. Proc, Fiftieth Workshop on Geothermal Reservoir Engineering Stanford University, Stanford, California.

Falko, V., Jörg, H., & Lars, R. (2021). Brine formation and mobilization in submarine hydrothermal systems: Insights from a novel multiphase hydrothermal flow model in the system H2O--NaCl. Transport in Porous Media, 136, 65--102.

Geiger, S., Driesner, T., Heinrich, C. A., & Matthäi, S. (2006a). Multiphase thermohaline convection in the earth's crust: I. A new finite element—Finite volume solution technique combined with a new equation of state for NaCl-H2O. Transport in Porous Media, 63(3), 399–434. https://doi.org/10.1007/s11242-005-0108-z

Geiger, S., Driesner, T., Heinrich, C. A., & Matthäi, S. (2006b). Multiphase thermohaline convection in the earth's crust: II. Benchmarking and application of a finite element—Finite volume solution technique with a NaCl-H2O equation of state. Transport in Porous Media, 63(3), 435–461. https://doi.org/10.1007/s11242-005-0109-y

Gharbia, I. B., Haddou, M., Tran, Q. H., & Vu, D. T. S. (2021). An analysis of the unified formulation for the equilibrium problem of compositional multiphase mixtures. Mathematical Modelling and Numerical Analysis. https://doi.org/10.1051/m2an/2021075

Guo, Z., & Rüpke, L. (2021). swEOS: multi-platform multi-language package of salt-water equation of state (Version 1.7.0) [C++]. https://doi.org/10.5281/zenodo.4603878

Guo, Z., Rüpke, L., & Tao, C. (2020). HydrothermalFoam v1.0: A 3-D hydrothermal transport model for natural submarine hydrothermal systems. Geoscientific Model Development Discussions, 13(12), 6547–6565. https://doi.org/10.5194/gmd-2020-140

Ingebritsen, S. E., Geiger, S., Hurwitz, S., Hurwitz, S., & Driesner, T. (2010). Numerical simulation of magmatic hydrothermal systems. Reviews of Geophysics, 48(1), 1002. https://doi.org/10.1029/2009rg000287

Keilegavlen, E., Berge, R. L., Fumagalli, A., Starnoni, M., Stefansson, I., Varela, J., & Berre, I. (2021). PorePy: An open-source software for simulation of multiphysics processes in fractured porous media. Computational Geosciences, 25, 243–265. https://doi.org/10.1007/s10596-020-10002-5

Khait, M. (2019). Delft Advanced Research Terra Simulator (DARTS): General purpose reservoir simulator with operator-based linearization. https://doi.org/10.4233/uuid:5f0f9b80-a7d6-488d-9bd2-d68b9d7b4b87

Kipp, K. L., Hsieh, P. A., Charlton, S. R., & Charlton, S. R. (2008). Guide to the revised ground-water flow and heat transport simulator: HYDROTHERM - Version 3. Techniques and Methods. https://doi.org/10.3133/tm6a25

Lauser, A., Hager, C., Helmig, R., & Wohlmuth, B. (2011). A new approach for phase transitions in miscible multi-phase flow in porous media. Advances in Water Resources, 34(8), 957–966. https://doi.org/10.1016/j.advwatres.2011.04.021

Les Landes, A. A., Beaude, L., Castanon Quirox, D., Jeannin, L., Lopez, S., Smaï, F., Guillon, T., & Masson, R. (2025). Geothermal modeling in complex geological systems with ComPASS. Computers & Geosciences, Elsevier, 194, 105752.

Lewis, K. C., & Lowell, R. P. (2009). Numerical modeling of two-phase flow in the NaCl-H2O system: Introduction of a numerical method and benchmarking. Journal of Geophysical Research, 114. https://doi.org/10.1029/2008jb006029

Lipovac, V., Duran, O., Keilegavlen, E., Radu, F., & Berre, I. (2023). Unified flash calculations with isenthalpic and isochoric constraints. Fluid Phase Equilibria, 113991–113991. https://doi.org/10.1016/j.fluid.2023.113991

Lopez, S., Masson, R., Beaude, L., Birgle, N., Brenner, K., Kern, M., Smaï, F., & Xing, F. (2018). Geothermal modeling in complex geological systems with the ComPASS code. Proceedings of the Stanford Geothermal Workshop.

Luis C. A, G.-N. (2024). Evolution of worldwide geothermal power 2020–2023. Geothermal Energy. https://doi.org/10.1186/s40517-024-00290-w

Podgorney, R., Huang, H., & Gaston, D. (2010). A fully-coupled, implicit, finite element model for simultaneously solving multiphase fluid flow, heat transport, and rock deformation. Geothermal Resources Council Annual Meeting 2010, Geothermal 2010.

Pruess, K. (1991). TOUGH2: A general-purpose numerical simulator for multiphase nonisothermal flows. Lawrence Berkeley National Lab.(LBNL), Berkeley, CA (United States). https://doi.org/10.2172/138333

Pruess, K. (2003). The TOUGH codes—A family of simulation tools for multiphase flow and transport processes in permeable media. Lawrence Berkeley National Laboratory. https://doi.org/10.2136/vzj2004.0738

Quiroz, D. C., Jeannin, L., Lopez, S., & Masson, R. (2024). Multi-segmented non-isothermal compositional liquid gas well model for geothermal processes. arXiv.Org. https://doi.org/10.48550/arxiv.2401.02406

Rajabi, M. M., & Chen, M. (2023). Dynamical modeling of a geothermal system to predict hot spring behavior. Modeling Earth Systems and Environment, 9(3), 3085–3093. https://doi.org/10.1007/s40808-023-01696-4

Reinsch, T., Asanuma, H., Huenges, E., Poletto, F., & Dobson, P. (2017). Utilizing supercritical geothermal systems: A review of pas ventures and ongoing research activities. Geothermal Energy. https://doi.org/10.1186/s40517-017-0075-y

Richter, A. (2023). ThinkGeoEnergy's Top 10 Geothermal Countries 2022–Power Generation Capacity (MW).

Sabine, F., Jana, S., Szolgayova, J., Michael, O., Obersteiner, M., & Gusti, M. (2008). Investment under market and climate policy uncertainty. Applied Energy, 85(8), 708–721. https://doi.org/10.1016/j.apenergy.2008.01.005

Voskov, D. (2017). Operator-based linearization approach for modeling of multiphase multi-component flow in porous media. Journal of Computational Physics, 337, 275–288. https://doi.org/10.1016/j.jcp.2017.02.041

Voskov, D., & Tchelepi, H. (2012). Comparison of nonlinear formulations for two-phase multi-component EoS based simulation. Journal of Petroleum Science and Engineering, 82, 101--111.

Wang, Y., Voskov, D., Khait, M., & Bruhn, D. (2020). An efficient numerical simulator for geothermal simulation: A benchmark study. Applied Energy, 264, 114693. https://doi.org/10.1016/j.apenergy.2020.114693

Weis, P., Driesner, T., Coumou, D., & Geiger, S. (2014). Hydrothermal, multiphase convection of H2O-NaCl fluids from ambient to magmatic temperatures: A new numerical scheme and benchmarks for code comparison. Geofluids, 14(3), 347–371. https://doi.org/10.1111/gfl.12080

Xia, Y., Podgorney, R., & Huang, H. (2017). Assessment of a hybrid continuous/discontinuous Galerkin finite element code for geothermal reservoir simulations. Rock Mechanics and Rock Engineering, 50(3), 719–732. https://doi.org/10.1007/s00603-016-0951-y

Zyvoloski, G., Robinson, B. A., Dash, Z. V., & Trease, L. L. (1997). Summary of the models and methods for the FEHM application-a finite-element heat-and mass-transfer code. Los Alamos National Lab.(LANL), Los Alamos, NM (United States). https://doi.org/10.2172/14903